# Computational screening of two-dimensional coatings for semiconducting photocathodes

Gaoxue Wang, Ping Yang, and Enrique R. Batista

Phys. Rev. Materials **4**, 024001 — Published 26 February 2020

DOI: 10.1103/PhysRevMaterials.4.024001

# Computational screening of two-dimensional coatings for semiconducting photocathodes

Gaoxue Wang, Ping Yang*, and Enrique R. Batista*

Los Alamos National Laboratory, Los Alamos, NM 87544

(January 28, 2019)

*Corresponding author: erb@lanl.gov
pyang@lanl.gov

## Abstract

Alkali-based semiconducting photocathodes, due to their high quantum efficiency (QE) in the visible light spectrum, are promising candidates to replace traditional metal photocathodes for high-brightness beam applications such as X-ray free electron laser (XFEL). However, they suffer from rapid degradation which significantly limits their operational lifetimes. Coating them with two-dimensional (2D) materials has been proposed as a possible avenue to prevent the degradation. Ideally, the 2D coating layer should not increase the work function of semiconducting photocathodes, thus maintaining the high QE of semiconducting photocathodes in the visible light. Herein, we report a computational screening of over 4000 2D materials in the Computational 2D Materials Database (C2DB). The assessment of their potential to be good coating layers is based on their effects to the surface electronic properties. We discover several candidate materials that are even capable of decreasing the work function of semiconducting photocathodes. Some of the experimentally synthesized 2D materials, such as hydrogenated graphene (graphane) and several hydroxylated transition metal carbides/nitrides (MXenes) are particularly appealing for this application.

**Keywords:** photocathodes, 2D materials, work function, computational screening

## I. INTRODUCTION

Photocathodes play a key role in electron accelerators for future light sources, such as X-ray free electron laser (XFEL) and X-ray energy recovery linacs (XERL) [1]. Alkali-based semiconducting photocathodes such as cesium antimony ($Cs_3Sb$) and bialkali antimony ($K_2CsSb$) have high quantum efficiency (QE) at the level of 1~20% in the visible light [2,3], making them prime candidates to replace metallic photocathodes for generating high brightness electron beams [4]. However, these Cs-based semiconducting photocathodes are extremely reactive, particularly with respect to oxygen-containing residual gas molecules even in the ultra-high vacuum (UHV) conditions inside the accelerators, resulting in much shorter operational lifetimes than their metallic counterparts [3,5-9].

Coating with inert two-dimensional (2D) materials is a conceptually attractive approach to improve the lifetimes of semiconducting photocathodes as schematically shown in Figure 1(a) [10-12]. In a previous study, we showed how a few layers of hexagonal boron nitride (*h*-BN) can overcome the QE-lifetime tradeoff of alkali-based semiconducting photocathodes [13]. *h*-BN exhibits excellent chemical stability, thus presenting a chemical barrier to prevent the degradation of semiconducting photocathodes from the reactions with residual gases; at the same time, *h*-BN can decrease the work function, thus maintain the high QE of semiconducting photocathodes in the visible light spectrum. While other popular 2D materials studied, graphene and $MoS_2$ increase the work function and shift the photoelectric threshold towards the ultraviolet spectrum, resulting in significant reduction of the QE in the visible spectrum. This difference between BN and graphene/$MoS_2$ was identified to originate from their band alignment with the photocathodes: the conduction band minimum (CBM) of $MoS_2$ or the Fermi level of graphene is lower than the Fermi level of the photocathodes. This leads to the electron transfer from photocathodes to the coating layers, thus the formation of inward pointing interfacial dipoles that present extra energy barriers for the outward going electrons. In contrast, the CBM of *h*-BN is higher than the Fermi level of the photocathodes, which prevents such electron transfer. Therefore, the band alignment between the photocathodes and the coating layer, as shown in shown in Figure 1(b), is a crucial criterion for selecting 2D coatings for semiconducting photocathodes [13].

Whereas the experimental approach for finding a suitable coating material is time consuming and less efficient than direct calculation of the physical properties of materials, computational high-throughput screening is getting increasingly popular in materials science thanks to the availability of large material datasets. In this letter, we have screened in the Computational 2D Materials Database (C2DB) [14] for suitable 2D coating materials for alkali-based semiconducting photocathodes. Several candidate materials besides *h*-BN have been discovered. Especially hydrogenated graphene (graphane), hydrogenated silicon-carbon, hydrogenated germanium-carbon, and several hydroxylated transition metal carbides/nitrides (MXenes) were identified to be promising for this application. The results are important for the development of robust photocathodes for future applications.

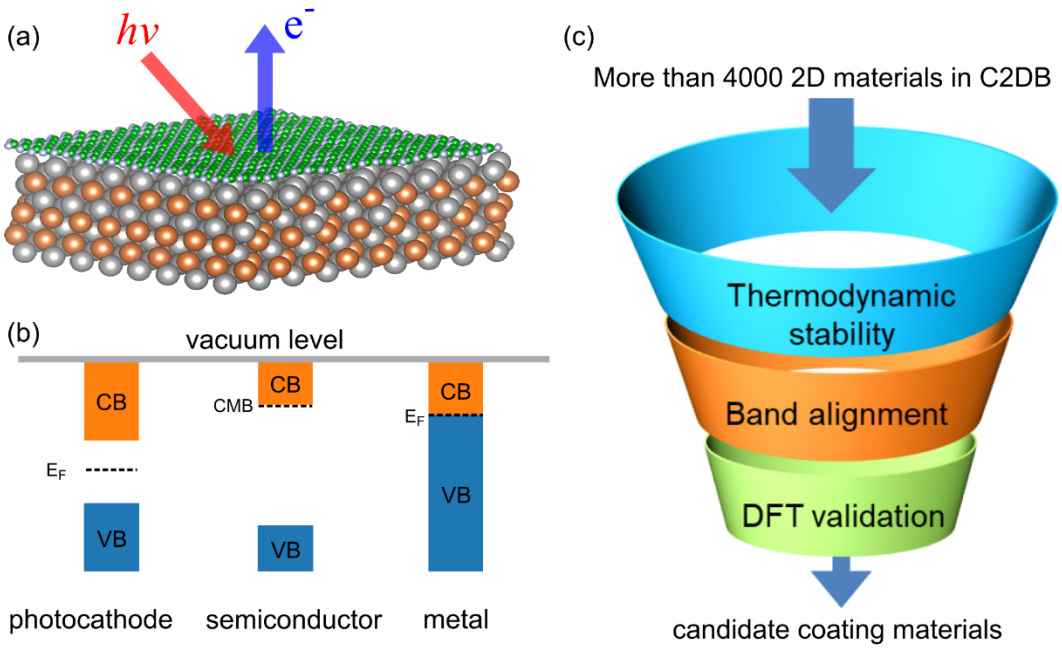


*Figure 1. (a) Schematic illustration of passivating photocathodes with a 2D coating layer, (b) band alignment of semiconducting photocathodes and an ideal semiconducting or metallic coating material, and (c) the computaitonal screening strategy in the C2DB. CB (VB) respresents the conduction band (valence band), and $E_F$ is the Fermi level.*

## II. METHODS

*Electronic structure calculations*

Our calculations were performed with the use of density functional theory (DFT) and projector augmented-wave (PAW) method [15] as implemented in the Vienna *ab initio* Simulation Package (VASP) [16]. The generalized gradient approximation (GGA) of Perdew-Burke-Ernzerhof (PBE) [17] functional was used to represent the exchange-correlation interaction. Since PBE functional could not capture the van der Waals (vdW)

[18,19], the DFT-D3 method of Grimme [20] was included in the calculations. Plane wave basis sets with a cutoff energy of 500 eV were employed [15]. The energy convergence was set to $10^{-6}$ eV and the residual force on each atom was smaller than 0.01 eV/Å for structural relaxations. The surfaces of photocathodes were represented with slab models with a vacuum gap in the direction normal to the surface. In the supercell, the vacuum distance normal to the slab was larger than 30 Å to eliminate the interactions between the replicas due to the periodic boundary conditions. The Brillouin zone of the supercell was sampled by a uniform Monkhorst-Pack *k*-point grid [21]. The dipole correction was included to nullify the artificial field imposed on the slab by the periodic boundary conditions [22]. The surfaces were terminated with alkali atoms, which were the most stable surface configurations according to our previous work [9]. The change of work function was also checked with DFT calculations using HSE06 hybrid functional [23].

*Screening strategy for 2D coatings*

The overall screening strategy is illustrated in Figure 1(c). The first screening of 2D materials in the C2DB was based on two criteria identified from our previous study [13]: i) band alignment, and ii) thermodynamic and dynamic stability. As mentioned in the previous section, the band alignment between the photocathode and the coating layer plays a critical role. The lowest empty electronic state of the coating layer should be higher than the Fermi level of the photocathode (Figure 1(b)). The computed work function of alkali-antimonide photocathodes is in the range of 2-3 eV depending on the facets [13], which is in agreement with the experiments [24]. Therefore, we have employed the criterion of CBM > -2.0 eV for screening semiconducting 2D materials, and Fermi level > -2.0 eV for metallic 2D materials. Note that the energy levels are relative to the vacuum level that is set to 0 eV. For the second criteria, there are more than 4000 2D materials in the C2DB, some of the materials may be less stable and difficult to be synthesized in the free-standing forms. We therefore have followed the stability criteria in the work by Haastrup *et al.* [14], and only considered materials that are labeled to have a high/medium thermodynamic and dynamic stability (heat of formation < 0.2 eV/atom, minimum eigenvalue of the dynamical matrix > -2.0 eV/Å$^2$, and diagonal elements of the elastic constants $C_{ii}$ > 0 GPa). Note the procedure to determine the stability in C2DB provides a necessary, but not sufficient condition for the dynamic stability of 2D materials. A rigorous test for the stability requires the

calculation of full phonon band structure and elastic stiffness $C_{ij}$ [25]. 2D materials that can pass these two screening criteria are further validated using DFT calculations to ensure that they can provide protection, while not significantly increasing the work function of semiconducting photocathodes.

## III. RESULTS AND DISCUSSION

*Identified 2D coatings*

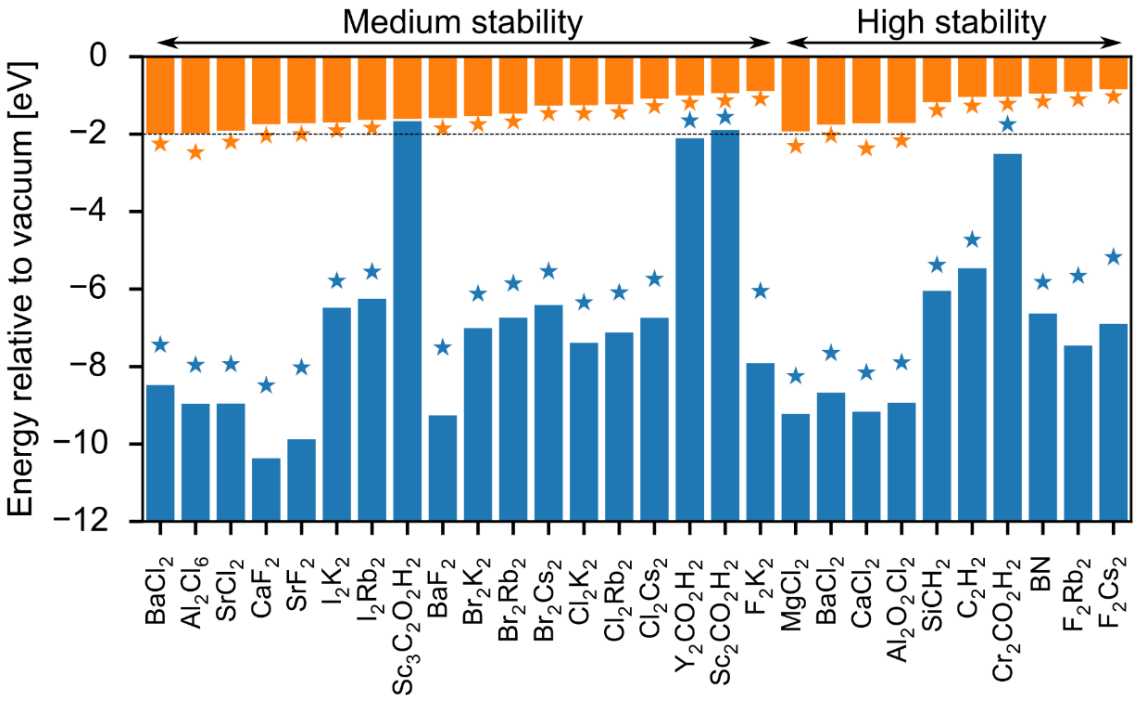


*Figure 2. Energy levels of semiconducting photocathodes screened from the C2DB. The stars are the energy levels calculated from PBE functional, and bars are from the hybrid functional HSE06.*

From the over 4000 materials in C2DB, 28 semiconducting 2D materials were identified to have a CBM higher than -2.0 eV at HSE06 level of theory. Their energy levels are shown in Figure 2. Interestingly, the CBM calculated with the PBE functional is in good agreement to the predictions of the HSE06 functional, whereas the VBM from PBE functional is significantly higher than the results from HSE06 functional, opening the bandgap as expected for the hybrid DFT functional [26]. Among these materials, 10 of them have a high thermodynamic and dynamic stability (heat of formation < convex hull + 0.2 eV/atom, minimum eigenvalue of the dynamical matrix > -0.01 meV/Å$^2$, and $C_{ii} > 0$ GPa), including *h*-BN, chloride monolayers ($MgCl_2$, $BaCl_2$, $CaCl_2$, $Al_2O_2Cl_2$), hydrogenated monolayers (graphane, $SiCH_2$), one MXene ($Cr_2CO_2H_2$), and two alkali fluoride monolayers ($Cs_2F_2$, $Rb_2F_2$). The rest of the 2D

materials have a medium thermodynamic or dynamic stability. For metallic 2D materials, we identified 21 candidates with Fermi level higher than -2.0 eV. Their energy levels are shown in Figure 3. All the identified metallic 2D materials are hydroxylated MXenes. Among these, 5 have a high thermodynamic and dynamic stability, including $Mn_2NO_2H_2$, $V_2CO_2H_2$, $V_2NO_2H_2$, $Ti_2CO_2H_2$, and $Ti_4C_3O_2H_2$. The atomic configurations for these identified materials are provided in the Supporting Information [27].

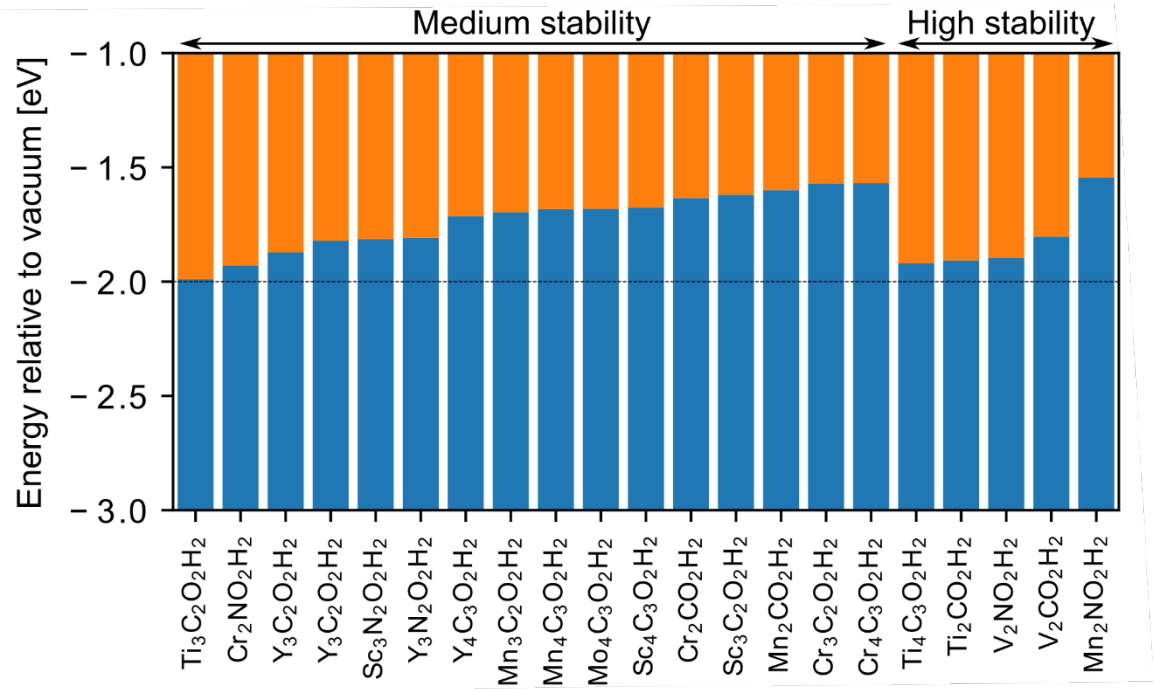


*Figure 3. Energy levels of metallic photocathodes screened from the C2DB.*

*DFT validation*

To further evaluate the identified 2D materials to be potential coatings, we calculated the change of work function of $Cs_3Sb$ upon coating with 2D materials. $Cs_3Sb$ is a well characterized semiconducting photocathodes [9]. We have selected some of the representative 2D materials with a high thermodynamic and dynamic stability in Figures 2 and 3, including semiconducting $C_2H_2$, $SiCH_2$, $Al_2O_2Cl_2$, $CaCl_2$, $Cr_2CO_2H_2$, $Cs_2F_2$ and metallic $Mn_2NO_2H_2$. Their atomic structures are shown in Figure 4.

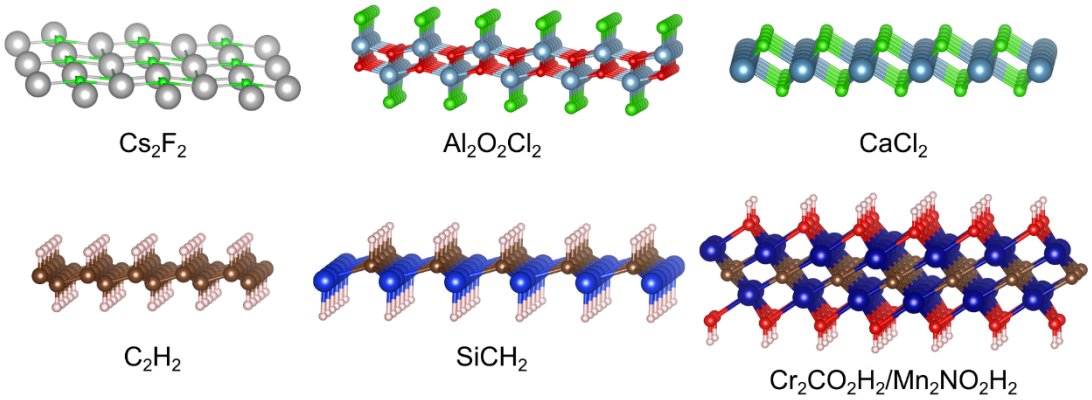


*Figure 4. Representative 2D coating materials for semiconducting photocathodes.*

Large supercells that minimize the lattice mismatch between $Cs_3Sb$ surfaces and the coating layers were used to calculate the properties of the coated surfaces, and all the atomic positions in the supercells were fully relaxed. The structure of uncoated $Cs_3Sb$ (111) surface, and the surface after coating with $SiCH_2$ and $Mn_2N_2OH_2$ are plotted in Figure 5. The remaining relaxed structures are shown in Figure S1 in the Supporting Information [27]. The work function is calculated as $WF = E_{vac} - E_F$, where $E_{vac}$ is the planar averaged electrostatic potential in the vacuum region, and $E_F$ is the Fermi energy as illustrated in Figures 6(a) and 6(c). The calculated work function of uncoated $Cs_3Sb$ (111) and (100) surfaces is 2.05 eV and 2.01 eV, respectively, which are in good agreement with the experimental results of 2.1 eV [24].

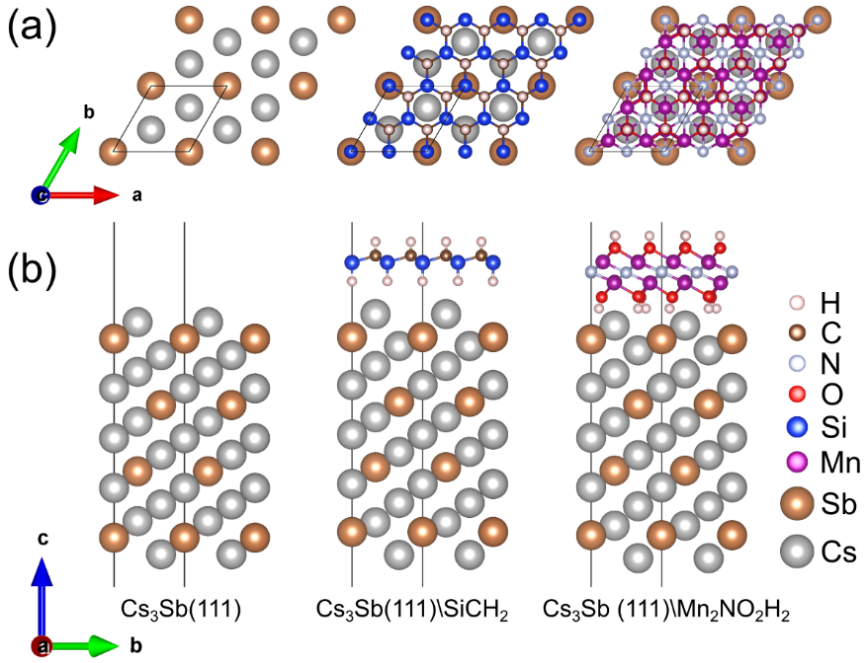


*Figure 5. Top views (a) and side views (b) of uncoated $Cs_3Sb$ (111) surface, and $SiCH_2$ (Si-closer configuration), $Mn_2NO_2H_2$ coated $Cs_3Sb$ (111) surfaces, respectively.*

The change of work function ($\Delta WF = WF_{\text{coated}} - WF_{\text{uncoated}}$) of $Cs_3Sb$ surfaces upon coating with these 2D materials is summarized in Table 1. Several materials were found to decrease the work function, which can lower the barrier for electrons to leave the surface, in effect of enhancing the QE. Notably, $SiCH_2$ (Si-closer configuration, Figures 6(a) and 6(b)) decreases the work function as much as -0.98 eV at GGA-PBE level of theory, that is even larger than what we had previously found for *h*-BN (-0.4 eV). This is attributed to the buckled structure of $SiCH_2$, as seen in Figures 4 and 5, leading to an intrinsic dipole moment pointing from the Si side to the C side. As seen from the band structure in Figure 6(b), the Fermi level of the $Cs_3Sb$\$SiCH_2$ hybrid structure is below the CBM of $SiCH_2$ indicating there is no electron transfer from $Cs_3Sb$ to $SiCH_2$. In contrast to the Si-closer configuration, coating with the C-closer configuration increases the work function by 1.8 eV. We have also considered the isoelectronic $GeCH_2$ (Ge-closer configuration) with an identical structure to $SiCH_2$. It has a similar effect of decreasing the work function by -0.96 eV.

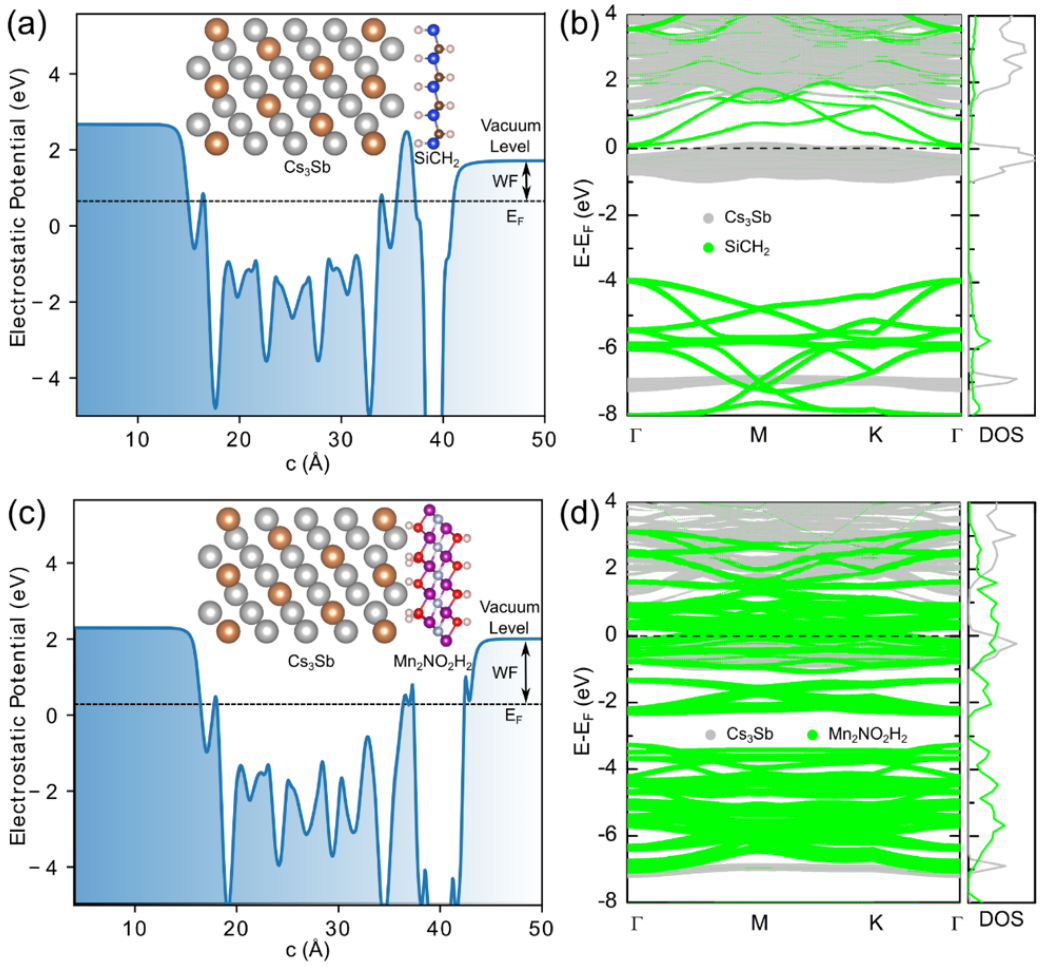


*Figure 6. Planar averaged electrostatic potentials (a,c) and electronic band structures (b,d) of $SiCH_2$ and $Mn_2NO_2H_2$ coated $Cs_3Sb$ (111) surface.*

Compared to graphene that increases the work function by 1.5 eV, the hydrogenated version (graphane or $C_2H_2$), is much less intrusive in the electronic properties of the surface, slightly increasing the work function by 0.12 eV using GGA-PBE functional. The binding energy of the coating layer on photocathodes is defined as $E_{\mathrm{b}} = E_{\mathrm{surface+coating}} - (E_{\mathrm{surface}} + E_{\mathrm{coating}})$, where $E_{\mathrm{surface+coating}}$, $E_{\mathrm{surface}}$ and $E_{\mathrm{coating}}$ are the total energies of the complex, the uncoated surface, and the coating layer, respectively. For the hydrogenated monolayers including $C_2H_2$ and $SiCH_2$, the binding energies are in the range -7.0 meV/Å$^2$ to -10 meV/Å$^2$, which are close to the interlayer interactions of graphite (-11.8 meV/Å$^2$) [28], indicating that the hydrogenated monolayers can be attached to the surface of photocathodes through weak van der Waals (vdW) interaction. It should be noted that graphane has been synthesized by hydrogenation of graphene [29,30]. Our work predicts new application of graphane as a coating layer for semiconducting photocathodes.

*Table 1. Size of the supercell and k-point grid, binding energy $E_b$, and change of work function $\Delta WF$ at PBE and HSE06 level of theory for various 2D materials on $Cs_3Sb$ (111) or (100) surface.*

| 2D materials | | Supercell size (Å$^2$) | *k*-point grid | $E_{\mathrm{b}}$ (meV/Å$^2$) | $\Delta WF_{\mathrm{PBE}}$ (eV) | $\Delta WF_{\mathrm{HSE06}}$ (eV) |
|---|---|---|---|---|---|---|
| | *h*-BN | 12.55×13.04<br>**12.95×12.95 (100)** | 3×3×1 | -9.02 | -0.40 [13] | -0.81 |
| | graphane ($C_2H_2$) | 12.69×12.69<br>**12.95×12.95 (111)** | 3×3×1 | -8.16 | +0.12 | +0.06 |
| | $SiCH_2$ (Si-closer) | 6.26×6.26<br>**6.48×6.48 (111)** | 7×7×1 | -8.31 | -0.98 | -1.21 |
| | $SiCH_2$ (C-closer) | 6.26×6.26<br>**6.48×6.48 (111)** | 7×7×1 | -7.66 | +1.80 | +1.83 |
| | $GeCH_2$ (Ge-closer) | 6.50×6.50<br>**6.48×6.48 (111)** | 7×7×1 | -7.66 | -0.96 | -1.26 |
| | $Cr_2CO_2H_2$ | 6.14×6.14<br>**6.48×6.48 (111)** | 7×7×1 | -48.24 | -0.48 | +0.02 |
| | $Al_2O_2Cl_2$ | 18.37×6.35<br>**19.42×6.48 (100)** | 3×7×1 | -14.61 | +0.44 | +0.09 |
| | $CaCl_2$ | 12.41×12.41<br>**12.95×12.95 (111)** | 3×3×1 | -13.56 | +1.16 | +0.92 |
| | $Cs_2F_2$ | 5.77×5.77<br>**6.48×6.48 (100)** | 7×7×1 | -205.36 | -0.54 | -0.69 |
| Metal | graphene | 12.35×12.83<br>**12.95×12.95 (100)** | 3×3×1 | -24.3 | +1.50 [13] | +1.60 |
| | $Mn_2NO_2H_2$ | 6.14×6.14<br>**6.48×6.48 (111)** | 7×7×1 | -34.21 | -0.29 | -0.34 |

MXenes are a large family of 2D materials [31-33]. Different methods to functionalize MXenes, such as hydroxylation, have been realized by several groups recently [34-39]. Our calculations yielded that semiconducting $Cr_2CO_2H_2$, and metallic $Mn_2NO_2H_2$

(Figures 6(c) and 6(d)) decrease the work function by -0.48 and -0.29 eV at GGA-PBE level of theory, respectively. The binding energies of $Cr_2CO_2H_2$ and $Mn_2NO_2H_2$ are -48.24 and -34.21 meV/Å$^2$, respectively. The reduction of work function and negative binding energies of $Cr_2CO_2H_2$ and $Mn_2NO_2H_2$ indicate they are good coatings for semiconducting photocathodes. Since other hydroxylated MXenes that are identified in Figures 2 and 3 share similar atomic and electronic structures with $Cr_2CO_2H_2$ or $Mn_2NO_2H_2$, they are expected to be good coatings as well.

$Cs_2F_2$ decreases the work function by -0.54 eV and binds strongly on the $Cs_3Sb$ surface with a binding energy of -205.36 meV/Å$^2$ at GGA-PBE level of theory. Since $Cs_2F_2$, $Rb_2F_2$, $K_2F_2$, $Cs_2Cl_2$, $Rb_2Cl_2$, $K_2Cl_2$, $Cs_2Br_2$, $Cs_2I_2$ and $Cs_2I_2$ have similar semiconducting properties and their CBM are all above the Fermi level of $Cs_3Sb$ (Figure 2), forming thin alkali-halide films on alkali-based semiconducting photocathodes is expected to provide protection without decreasing the QE. In fact, previous experiments have demonstrated that alkali-halide coatings can be used to activate and increase the stability of semiconducting photocathodes [40,41].

The chloride monolayers, $CaCl_2$ and $AlO_2Cl_2$, were found to increase the work function significantly by 1.16 and 0.44 eV, respectively. We noticed that the $CaCl_2$ structure was severely distorted upon coating on $Cs_3Sb$ forming strong Cs-Cl and Ca-Sb bonds (Figure S1 [27]). Therefore, $CaCl_2$ and $AlO_2Cl_2$ are unlikely to be good coatings for alkali-based photocathodes.

It is well-known that the band gaps of semiconductors are underestimated using GGA-PBE functional. We have also checked the change of work function with HSE06 hybrid functional [23] which is more reliable for predicting the electronic structure of semiconductors [26]. Due to the high computational cost of using HSE06, we limited the use of it to single-point calculations at the PBE optimized geometries. The corresponding $\Delta WF_{\mathrm{HSE06}}$ is shown in Table 1. It is seen that the difference in $\Delta WF_{\mathrm{HSE06}}$ and $\Delta WF_{\mathrm{PBE}}$ is smaller than 0.5 eV for all the structures. The selected hydrogenated monolayers including graphane, $SiCH_2$ (Si-closer), and $GeCH_2$ (Ge-closer), and hydroxylated MXenes $Cr_2CO_2H_2$ and $Mn_2NO_2H_2$ decrease or only slightly increase the work function at HSE06 level of theory, thus further validating the 2D materials identified through the procedure in this work to be promising coatings for semiconducting photocathodes.

## IV. CONCLUSIONS

In summary, we computationally screened out all the 2D materials in the C2DB dataset that can serve as coatings for alkali-based semiconducting photocathodes. Besides *h*-BN, two families of 2D materials are identified: i) Hydrogenated monolayers, graphane ($C_2H_2$), $SiCH_2$ and $GeCH_2$, and ii) Hydroxylated MXenes. Although graphene significantly increases the work function of alkali-based photocathodes, hydrogenated graphene (graphane) only slightly increases the work function. $SiCH_2$ and $GeCH_2$ monolayers can decrease the work function by around -1 eV due to their intrinsic dipole moments. Several metallic or semiconducting hydroxylated MXenes can decrease the work function of $Cs_3Sb$, suggesting this family of materials has bright future as protective coatings. Some of the identified materials have already been synthesized, such as graphane [29,30] and hydroxylated MXenes [31-39]. Bianco *et al.* have demonstrated that germanane, a germanium graphane analogue [42], only slowly oxidizes in air over the span of 5 months, indicating good degradation resistance of hydrogenated monolayers. Lipatov *et al.* have reported that hydroxylated MXenes have reasonable stability and remain their electronic properties even after exposure to air for more than 24 hours [43]. Considering the reduction of work function and the good degradation resistance, hydrogenated monolayers and hydroxylated MXenes are promising 2D coatings for semiconducting photocathodes. Our computational screening can guide the design of photocathodes with elongated lifetimes and high QE in the visible light spectrum for accelerator applications.


## Acknoledgements

The authors gratefully acknowledge funding for this project from the Laboratory Directed Research and Development program of Los Alamos National Laboratory (LANL) under project 20180007DR and 20190079DR. LANL is operated by Triad National Security, LLC, for the National Nuclear Security Administration of U.S. Department of Energy (Contract No. 89233218CNA000001). G.W. thanks the Director's Postdoc Fellow from LANL. The calculations were performed using EMSL (grid.436923.9), a DOE Office of Science User Facility sponsored by the Office of Biological and Environmental Research.

## References


[1] P. Musumeci, J. G. Navarro, J. Rosenzweig, L. Cultrera, I. Bazarov, J. Maxson, S. Karkare, and H. Padmore, Nucl. Instrum. Methods Phys. Res., Sect. A **907**, 209-220 (2018).
[2] R. Xiang and J. Teichert, Phys. Procedia **77**, 58 (2015).
[3] P. Michelato, Nucl. Instrum. Methods Phys. Res., Sect. A **393**, 455 (1997).
[4] B. E. Carlsten, E. R. Colby, E. H. Esarey, M. Hogan, F. X. Kartner, W. S. Graves, W. P. Leemans, T. Rao, J. B. Rosenzweig, C. B. Schroeder, D. Sutter, and W. E. White, Nucl. Instrum. Methods Phys. Res., Sect. A **622**, 657 (2010).
[5] V. Pavlenko, F. Liu, M. A. Hoffbauer, N. A. Moody, and E. R. Batista, AIP Adv. **6**, 115008 (2016).
[6] L. R. Danielson, C. Lee, and P. E. Oettinger, Appl. Surf. Sci. **16**, 257 (1983).
[7] S. Pastuszka, A. S. Terekhov, and A. Wolf, Appl. Surf. Sci. **99**, 361 (1996).
[8] D. Durek, F. Frommberger, T. Reichelt, and M. Westermann, Appl. Surf. Sci. **143**, 319 (1999).
[9] G. Wang, R. Pandey, N. A. Moody, and E. R. Batista, J. Phys. Chem. C **121**, 8399 (2017).
[10] H. Yamaguchi, F. Liu, J. DeFazio, C. Villarrubia, D. Finkenstadt, K. L.Jensen, V. Pavlenko, M. Mehl, S. Lambrakos, G. Gupta, A. D. Mohite, and N. A. Moody, npj 2D Mater. Appl. **1**, 12 (2017).
[11] F. Liu, N. A. Moody, K. L. Jensen, V. Pavlenko, C. W. Narvaez Villarrubia, A. D. Mohite, and G. Gupta, Appl. Phys. Lett. **110**, 041607 (2017).
[12] H. Yamaguch, F. Liu, J. DeFazio, M. Gaowei, C. W. N. Villarrubia, J. Xie, J. Sinsheimer, D. Strom, V. Pavlenko, K. L. Jensen, J. Smedley, A. D. Mohite, and N. A. Moody, Adv. Mater. Interfaces **5**, 1800249 (2018).
[13] G. Wang, P. Yang, N. A. Moody, and E. R. Batista, npj 2D Mater. Appl. **2**, 17 (2018).
[14] S. Haastrup, M. Strange, M. Pandey, T. Deilmann, P. S. Schmidt, N. F. Hinsche, M. N. Gjerding, D. Torelli, P. M. Larsen, A. C. Riis-Jensen, J. Gath, K. W. Jacobsen, J. J. Mortensen, T. Olsen, and K. S. Thygesen, 2D Mater. **5**, 042002 (2018).
[15] G. Kresse and D. Joubert, Phys. Rev. B **59**, 1758 (1999).
[16] G. Kresse and J. Furthmüller, Comput. Mater. Sci. **6**, 15 (1996).
[17] J. P. Perdew, K. Burke, and M. Ernzerhof, Phys. Rev. Lett. **77**, 3865 (1996).
[18] B. Sachs, T. Wehling, M. Katsnelson, and A. Lichtenstein, Phys. Rev. B **84**, 195414 (2011).
[19] G. Giovannetti, P. A. Khomyakov, G. Brocks, P. J. Kelly, and J. Van Den Brink, Phys. Rev. B **76**, 073103 (2007).
[20] S. Grimme, J. Comput. Chem. **27**, 1787 (2006).
[21] H. J. Monkhorst and J. D. Pack, Phys. Rev. B **13**, 5188 (1976).
[22] L. Bengtsson, Phys. Rev. B **59**, 12301 (1999).
[23] J. Heyd, G. E. Scuseria, and M. Ernzerhof, J. Chem. Phys. **118**, 8207 (2003).
[24] J. Teichert, R. Xiang, G. Suberlucq, and J. W. Verschuur, CARE Note-2004-033-PHIN, http://esgard. lal. in2p3. fr/Project/Activities/Current/Deliverables/CARE_Deliverables.htm (2004).
[25] F. Mouhat and F.-X. Coudert, Phys. Rev. B **90**, 224104 (2014).
[26] J. Heyd, J. E. Peralta, G. E. Scuseria, and R. L. Martin, J. Chem. Phys. **123**, 174101 (2005).
[27] See Supplemental Material at [URL] for the coordinates of selected 2D materials and some of the relaxed surfaces.
[28] Z. Liu, J. Z. Liu, Y. Cheng, Z. Li, L. Wang, and Q. Zheng, Phys. Rev. B **85**, 205418 (2012).
[29] D. C. Elias, R. R. Nair, T. M. G. Mohiuddin, S. V. Morozov, P. Blake, M. P. Halsall, A. C. Ferrari, D. W. Boukhvalov, M. I. Katsnelson, A. K. Geim, and K. S. Novoselov, Science **323**, 610 (2009).
[30] M. Pumera and C. H. A. Wong, Chem. Soc. Rev. **42**, 5987 (2013).
[31] J. Halim, S. Kota, M. R. Lukatskaya, M. Naguib, M. Zhao, E. J. Moon, J. Pitock, J. Nanda, S. J. May, Y. Gogotsi, and M. W. Barsoum, Adv. Funct. Mater. **26**, 3118 (2016).
[32] M. Naguib, J. Come, B. Dyatkin, V. Presser, P.-L. Taberna, P. Simon, M. W. Barsoum, and Y. Gogotsi, Electrochem. Commun. **16**, 61 (2012).
[33] B. Anasori, Y. Xie, M. Beidaghi, J. Lu, B. C. Hosler, L. Hultman, P. R. Kent, Y. Gogotsi, and M. W. Barsoum, ACS nano **9**, 9507 (2015).
[34] J. Zhou, X.-H. Zha, M. Yildizhan, P. Eklund, J. Xue, M. Liao, P. O. Persson, S. Du, and Q. Huang, ACS nano **13**,1195 (2019).
[35] Q. Peng, J. Guo, Q. Zhang, J. Xiang, B. Liu, A. Zhou, R. Liu, and Y. Tian, J. Am. Chem. Soc. **136**, 4113 (2014).
[36] X. Jiang, S. Liu, W. Liang, S. Luo, Z. He, Y. Ge, H. Wang, R. Cao, F. Zhang, Q. Wen, J. Li, Q. Bao, D. Fan and H. Zhang, Laser Photonics Rev. **12**, 1700229 (2018).
[37] T. Li, L. Yao, Q. Liu, J. Gu, R. Luo, J. Li, X. Yan, W. Wang, P. Liu, B. Chen, W. Zhang, W. Abbas, R. Naz, and D. Zhang, Angew. Chem. Int. Ed. **57**, 6115 (2018).
[38] J. L. Hart, K. Hantanasirisakul, A. C. Lang, B. Anasori, D. Pinto, Y. Pivak, T. van Omme, S. J. May,

Y. Gogotsi, and M. L. Taheri, Nat. Commun. **10**, 522 (2019).
[39] T. Habib, X. Zhao, S. A. Shah, Y. Chen, W. Sun, H. An, J. L. Lutkenhaus, M. Radovic, and M. J. Green, npj 2D Mater. Appl. **3**, 8 (2019).
[40] T. Kaisheng, J. Electron. **5**, 53 (1988).
[41] E. Shefer, A. Breskin, T. Boutboul, R. Chechik, B. Singh, H. Cohen, and I. Feldman, J. Appl. Phys. **92**, 4758 (2002).
[42] E. Bianco, S. Butler, S. Jiang, O. D. Restrepo, W. Windl, and J. E. Goldberger, ACS Nano **7**, 4414 (2013).
[43] A. Lipatov, M. Alhabeb, M. R. Lukatskaya, A. Boson, Y. Gogotsi, and A. Sinitskii, Adv. Electron. Mater. **2**, 1600255 (2016).